Effects of magnetic field on the electronic structure of wurtzite quantum dots: Calculations using effective-mass envelope function theory

X. W. Zhang and J. B. Xia
Chinese Center of Advanced Science and Technology (World Laboratory), P.O. Box 8730, Beijing 100080, People's Republic of China and Institute of Semiconductors, Chinese Academy of Sciences, P.O. Box 912, Beijing 100083, People's Republic of China
(Received 9 May 2005; published 29 August 2005)

The Hamiltonian of the wurtzite quantum dots in the presence of an external homogeneous magnetic field is given. The electronic structure and optical properties are studied in the framework of effective-mass envelope function theory. The energy levels have new characteristics, such as parabolic property, antisymmtric splitting, and so on, different from the Zeeman splitting. With the crystal field splitting energy Δ_c=25 meV, the dark excitons appear when the radius is smaller than 25.85 Å in the absence of external magnetic field. This result is more consistent with the experimental results reported by Efros *et al.* [Phys. Rev. B **54**, 4843 (1996)]. It is found that dark excitons become bright under appropriate magnetic field depending on the radius of dots. The circular polarization factors of the optical transitions of randomly oriented dots are zero in the absence of external magnetic field and increase with the increase of magnetic field, in agreement with the experimental results. The circular polarization factors of single dots change from nearly 0 to about 1 as the orientation of the magnetic field changes from the x axis of the crystal structure to the z axis, which can be used to determine the orientation of the z axis of the crystal structure of individual dots. The antisymmetric Hamiltonian is very important to the effects of magnetic field on the circular polarization of the optical transition of quantum dots.

DOI: 10.1103/PhysRevB.72.075363 PACS number(s): 73.22.Dj, 75.90.+w, 78.67.Hc

I. INTRODUCTION

Ever since colloidal quantum dots were achieved, such nanostructures have become a major subject of attention because of their prospective application in devices. Xia[1,2] introduced the Baldereschi-Lipari[3] Hamiltonian to investigate the electronic structure of quantum dots.

Recently much attention has been paid to the optical properties of dots. Circular polarized emissions of quantum dots were observed in experiments.[4–7] Most of these experiments were done under magnetic field. Up to now, several different theoretical models have been used in the study of the electronic structure of dots under magnetic field. About 50 years ago, Luttinger[8] proposed the quantum theory of the cyclotron resonance in semiconductors. He introduced the symmetrized product and the antisymmetric Hamiltonian. Whaley *et al.*[9,10] calculated the g-factor of quantum dots using the tight-banding method. Early on, Efros *et al.*[11] studied the effects of magnetic field within the framework of single-band effective-mass approximation. Recently, Efros *et al.*[12] studied the structure of the electron quantum size levels in the framework of the eight-band effective-mass model[13] at zero and weak magnetic fields. But until now, a useful theoretical model, taking into account all effects of magnetic field no matter how strong in the framework of the six-band effective-mass envelope function theory, has not yet been introduced.

In this paper, we introduce a theoretical model in the framework of the six-band effective-mass approximation, which takes into account spin-orbit coupling (SOC), spin-Zeeman splitting, and symmetric and antisymmetric Hamiltonians in the presence of external magnetic field. The remainder of this paper is organized as follows. In Sec. II we give the form of the Hamiltonian. Our numerical results and discussions are given in Sec. III. Finally, we draw a brief conclusion in Sec. IV.

II. MODEL AND CALCULATION

If we take the basic functions of the valence-band top as

$$|1,1\rangle = (1/\sqrt{2})(X+iY), \tag{1a}$$

$$|1,0\rangle = Z, \tag{1b}$$

$$|1,-1\rangle = (1/\sqrt{2})(X-iY), \tag{1c}$$

the effective-mass Hamiltonian[2] of the hole in the zero SOC and zero magnetic field case is written as

$$H_{h0} = \frac{1}{2m_0}\begin{pmatrix} P_1 & S & T \\ S^* & P_3 & S \\ T^* & S^* & P_1 \end{pmatrix}, \tag{2}$$

where

$$P_1 = \gamma_1 p^2 - \sqrt{\frac{2}{3}}\gamma_2 P_0^{(2)}, \tag{3a}$$

$$P_3 = \gamma_1' p^2 + 2\sqrt{\frac{2}{3}}\gamma_2' P_0^{(2)} + 2m_0\Delta_c, \tag{3b}$$

$$T = \eta P_{-2}^{(2)} + \delta P_2^{(2)}, \tag{3c}$$

$$T^* = \eta P_2^{(2)} + \delta P_{-2}^{(2)}, \tag{3d}$$

$$S = Ap_0 P_{-1}^{(1)} + \sqrt{2}\gamma_3' P_{-1}^{(2)}, \tag{3e}$$

TABLE I. Parameters for CdSe in the actual calculation.

m_x	m_z	γ_1	γ_2	γ_2'	η	γ_1'	γ_3'	A	λ(meV)	Δ_c(meV)
0.1756	0.1728	1.7985	0.7135	0.7970	1.4492	2.166	0.3779	0.6532	139.3	25

$$S^* = -Ap_0P_1^{(1)} - \sqrt{2}\gamma_3'P_1^{(2)}. \tag{3f}$$

$P^{(2)}$ and $P^{(1)}$ are the second- and first-order tensors of the momentum operator, respectively. $p_0=\sqrt{2m_0\Delta}$, $\Delta=40$ meV. The effective-mass parameters[2] for CdSe are given in Table I. The matrix elements of all tensors of operators in this paper are given in Appendix B. The SOC Hamiltonian is written as

$$H_{so} = \begin{pmatrix} -\lambda & 0 & 0 & 0 & 0 & 0 \\ 0 & 0 & 0 & \sqrt{2}\lambda & 0 & 0 \\ 0 & 0 & \lambda & 0 & -\sqrt{2}\lambda & 0 \\ 0 & \sqrt{2}\lambda & 0 & \lambda & 0 & 0 \\ 0 & 0 & -\sqrt{2}\lambda & 0 & 0 & 0 \\ 0 & 0 & 0 & 0 & 0 & -\lambda \end{pmatrix}. \tag{4}$$

Here, we take the basic functions as $|1,\ 1\rangle\uparrow$, $|1,\ 0\rangle\uparrow$, $|1,-1\rangle\uparrow$, $|1,\ 1\rangle\downarrow$, $|1,\ 0\rangle\downarrow$, and $|1,-1\rangle\downarrow$. The envelope functions are

$$\Psi_h = \sum_{M=m+1/2}\sum_{l,n} \begin{pmatrix} a_{l,n,m,\uparrow}C_{l,n}j_l(k_n^l r)Y_{l,m-1}(\theta,\phi) \\ b_{l,n,m,\uparrow}C_{l,n}j_l(k_n^l r)Y_{l,m}(\theta,\phi) \\ d_{l,n,m,\uparrow}C_{l,n}j_l(k_n^l r)Y_{l,m+1}(\theta,\phi) \\ a_{l,n,m,\downarrow}C_{l,n}j_l(k_n^l r)Y_{l,m}(\theta,\phi) \\ b_{l,n,m,\downarrow}C_{l,n}j_l(k_n^l r)Y_{l,m+1}(\theta,\phi) \\ d_{l,n,m,\downarrow}C_{l,n}j_l(k_n^l r)Y_{l,m+2}(\theta,\phi) \end{pmatrix}. \tag{5}$$

M is the z component of the total angular momentum. The effective-mass Hamiltonian of electron is written as

$$H_{e0} = \frac{p^2}{2m_a} - \frac{1}{2m_b}\sqrt{\frac{2}{3}}P_0^{(2)}, \tag{6}$$

where

$$\frac{1}{m_a} = \frac{1}{3}\left(\frac{2}{m_x} + \frac{1}{m_z}\right), \tag{7a}$$

$$\frac{1}{m_b} = \frac{1}{3}\left(\frac{1}{m_x} - \frac{1}{m_z}\right). \tag{7b}$$

We take the basic functions as $S\uparrow$ and $S\downarrow$; S is the Bloch state of the conduction-band bottom. The envelope functions are

$$\Psi_e = \sum_m \sum_{l,n} \begin{pmatrix} e_{l,n,m,\uparrow}C_{l,n}j_l(k_n^l r)Y_{l,m}(\theta,\phi) \\ e_{l,n,m,\downarrow}C_{l,n}j_l(k_n^l r)Y_{l,m}(\theta,\phi) \end{pmatrix}. \tag{8}$$

For simplicity, hereafter we assume that the external magnetic field is applied in the x-z plane of crystal structure. If θ is the angle between the orientation of the magnetic field and the z axis of the crystal structure, then the components of the magnetic field are $B_z=B\cos\theta$, $B_x=B\sin\theta$, and $B_y=0$. For quantum spheres, we can choose the symmetric gauge, so that the vector potential is written as

$$\mathbf{A} = \left(-\frac{1}{2}B_z y, \frac{1}{2}B_z x - \frac{1}{2}B_x z, \frac{1}{2}B_x y\right). \tag{9}$$

In the presence of external magnetic field, the momentum operator changes into $\mathbf{p}\Rightarrow\mathbf{p}+e\mathbf{A}$. Because the different components of $\mathbf{p}$ do not commute, then the $p_\alpha p_\beta$ terms in the Luttinger Hamiltonian are not symmetric. Luttinger[8] introduced the symmetrized product

$$\{p_\alpha p_\beta\} = \frac{1}{2}(p_\alpha p_\beta + p_\beta p_\alpha). \tag{10}$$

He divided the Luttinger Hamiltonian into two parts, the symmetric part and the antisymmetric part. The antisymmetric part is simply written as

$$H_{asym} = K\mu_B \mathbf{I}\cdot\mathbf{B}. \tag{11}$$

Hereafter we name it the antisymmetric Hamiltonian, which introduces antisymmetric splitting. Luttinger[8] gave the forms of the components of $\mathbf{I}$ as the basic functions are X, Y, and Z,

$$I_x = \begin{pmatrix} 0 & 0 & 0 \\ 0 & 0 & -i \\ 0 & i & 0 \end{pmatrix}, \tag{12a}$$

$$I_y = \begin{pmatrix} 0 & 0 & i \\ 0 & 0 & 0 \\ -i & 0 & 0 \end{pmatrix}, \tag{12b}$$

$$I_z = \begin{pmatrix} 0 & -i & 0 \\ i & 0 & 0 \\ 0 & 0 & 0 \end{pmatrix}. \tag{12c}$$

If we take the basic functions as $|1,\ 1\rangle$, $|1,\ 0\rangle$, and $|1,\ -1\rangle$, the matrices change into

$$I_x = \begin{pmatrix} 0 & -\frac{\sqrt{2}}{2} & 0 \\ -\frac{\sqrt{2}}{2} & 0 & \frac{\sqrt{2}}{2} \\ 0 & \frac{\sqrt{2}}{2} & 0 \end{pmatrix}, \tag{13a}$$

$$I_y = \begin{pmatrix} 0 & \frac{\sqrt{2}}{2}i & 0 \\ -\frac{\sqrt{2}}{2}i & 0 & -\frac{\sqrt{2}}{2}i \\ 0 & \frac{\sqrt{2}}{2}i & 0 \end{pmatrix}, \tag{13b}$$

$$I_z = \begin{pmatrix} 1 & 0 & 0 \\ 0 & 0 & 0 \\ 0 & 0 & -1 \end{pmatrix}. \tag{13c}$$

The whole Hamiltonians of the electron and hole are respectively

$$H_e = H_{e0} + H_{mm\_e} + H_{Zeeman\_e}, \tag{14}$$

$$H_h = H_{h0} + H_{so} + H_{mm\_h} - H_{asym} - H_{Zeeman\_h}. \tag{15}$$

Hereafter we take the negative hole energy as positive. The terms H_{mm_e}, H_{mm_h}, H_{Zeeman_e}, and H_{Zeeman_h} are given in Appendix A.

III. RESULTS AND DISCUSSIONS

We calculated the electronic structure and optical properties of wurtzite quantum dots in the presence of external magnetic field. The unit of energy is

$$\varepsilon_0 = \frac{1}{2m_0}\left(\frac{\hbar}{R}\right)^2. \tag{16}$$

We use the dimensionless magnetic field

$$b = \frac{\hbar eB}{m_0 \varepsilon_0}. \tag{17}$$

A. Electronic states

The energies of the electron states of CdSe quantum spheres with any radius as functions of b when $\cos\theta=1$ are shown in Fig. 1(a). We do not take into account the spin Zeeman splitting as it is very simple. As we use the energy unit ε_0, the energy levels are independent of the radius. The symbol of each energy level represents the main components of its wave function. For example, (1, 0, 0) means that the state consists mainly of the $n=1$, $l=0$, $m=0$ state of the effective-mass envelope function multiplied with the S Bloch state of the conduction-band bottom. At $b=0$, the energies of the states with different $|m|$ and same n, l split. The energies of the states with bigger $|m|$ are lower. This is because of the second-order tensor of the momentum operator in the effective-mass Hamiltonian of the electron. If $m_x=m_z$, then the energy levels with different $|m|$ and same n, l are degenerate, due to the second term in Eq. (6) equal to zero. In the case of CdSe the m_x and m_z differ little as shown in Table I, so that the splitting of energy levels with different $|m|$ is very small, as shown in Fig. 1(a). As b increases, the energies split further due to the $m\cdot b$ terms in H_{mm_e}. The energies of the states with bigger m are higher. The energy levels have parabolic property due to the quadratic terms of b in H_{mm_e}. The energies of the electron states of CdSe quantum spheres with any radius as functions of b when $\cos\theta=1/2$ are shown in Fig. 1(b). The spin Zeeman splitting is also ignored. Compared with Fig. 1(a), We see that the energy levels almost do not change. The states mix up due to the magnetic field component perpendicular to the z axis of the crystal structure.

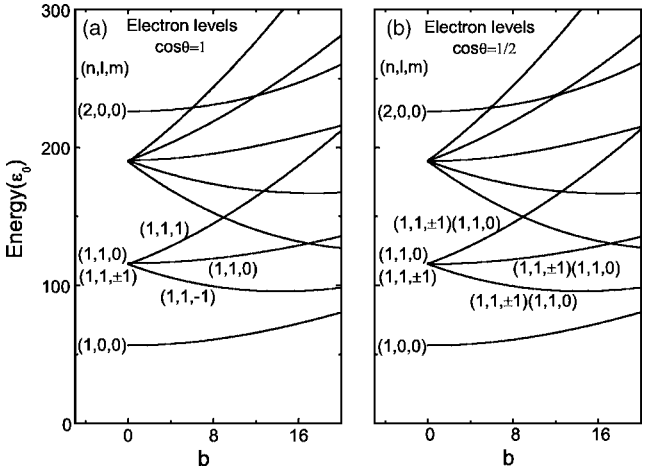

FIG. 1. (a) Energies of electron states of quantum dots as functions of b ($\cos\theta=1$). (b) Energies of electron states of quantum dots as functions of b ($\cos\theta=1/2$).

B. Hole states

The energies of the hole states of CdSe quantum sphere with radius of 21 Å as functions of b for $M=-3/2,-1/2,1/2,3/2$ are shown in Fig. 2. Here we assume that the external magnetic field is applied along the z axis of the crystal structure. As we choose the symmetric gauge, M is a good quantum number. The energy levels are dependent on the radius as we use the energy unit ε_0 due to the SOC Hamiltonian and the crystal field splitting energy Δ_c. The calculation by Whaley *et al.*[9] shows that the g-factors of the hole of CdSe quantum dots are nearly 2. So here and later we use $K_z=1$ and $g_{hz}=2$ for simplicity. The symbol of each energy level represents the main components of its wave function. For example, $S_{x+1}\uparrow$ means that the state consists mainly of the $n=1$, $l=0$ state of the effective-mass envelope function multiplied with the $|1, 1\rangle$ Bloch state of the valence-band top and the spin-up state. Then we see that the energies of the states with $M=\pm 1/2$ and $M=\pm 3/2$, which are degenerate at $b=0$, split as b increases, due to spin Zeeman splitting, antisymmetric splitting, and the b and b^2 terms in H_{mm_h}. The lowest energy levels of the states with $M=1/2,3/2$ go down in comparision with those of the states with $M=-1/2,-3/2$. The energy levels have a parabolic property due to the b^2 terms in H_{mm_h}.

The lowest two levels of the hole states are shown in Fig. 3(a) to see the details. It is interesting to notice that, at $b=0$, the hole ground state is optically passive, which is in agreement with the dark exciton theory.[11] Actually, at $b=0$, when the radius is smaller than 25.85 Å, there are dark ex-

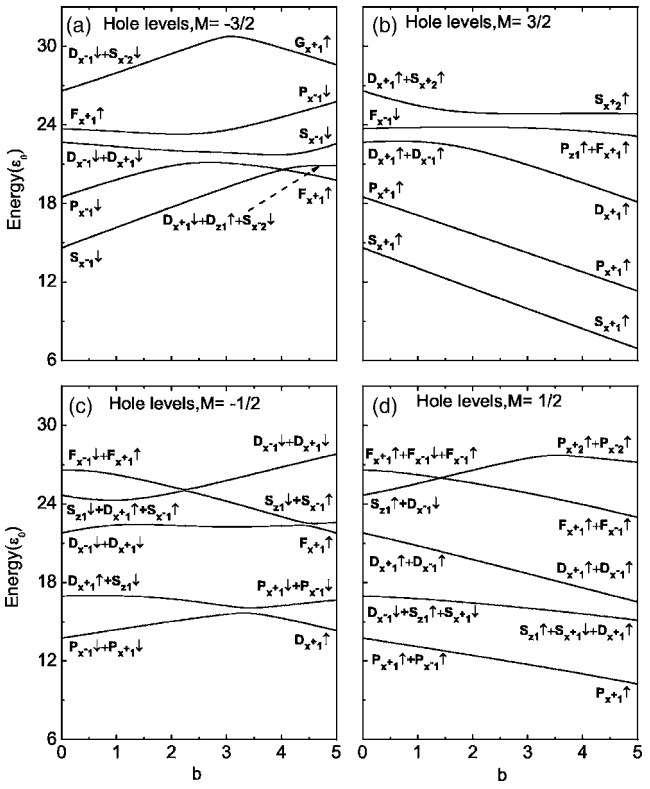

FIG. 2. Energies of hole states of quantum dots (21 Å) as functions of b. (a) $M=-3/2$. (b) $M=3/2$. (c) $M=-1/2$. (d) $M=1/2$.

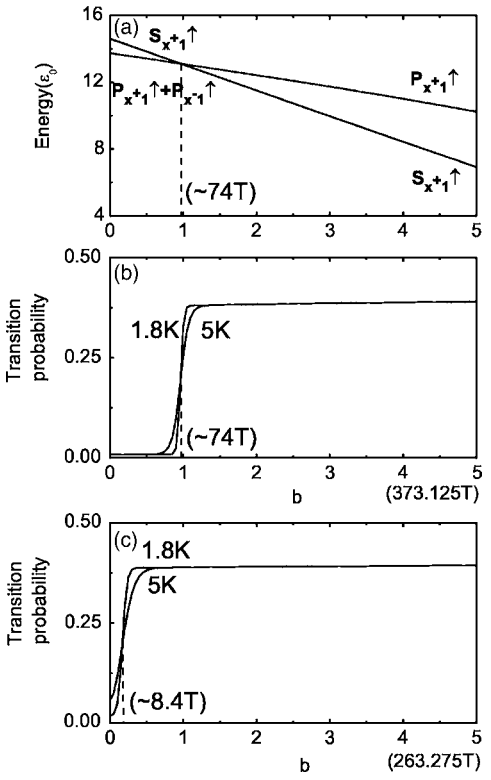

FIG. 3. (a) The lowest two energy levels of hole states of quantum dots (21 Å) as functions of b. (b) Transition probabilities of dots (21 Å) as functions of b. (c) Transition probabilities of dots (25 Å) as functions of b.

citons. The critical radius is smaller than 30 Å calculated by Xia,[2] because we use $\Delta_c=25$ meV, different from 40 meV used by Xia.[2] But when $b\gtrsim 1$, the hole ground state changes into $S_{x^+1}\uparrow$ with $M=3/2$, which is optically active. With the optical transition between a given electron state and a given hole state, the transition probability is proportional to $\{\Sigma_{l,n,m,s}[a_{l,n,m,s}e_{l,n,m,s}+d_{l,n,m,s}e_{l,n,m,s}+b_{l,n,m,s}e_{l,n,m,s}]\}^2$, and s represents the spin state, $\uparrow$ or $\downarrow$. Multiply the Boltzmann distribution factor of each state and sum up all the contributions to the transition probability. The transition probabilities at different temperatures as functions of b are shown in Fig. 3(b). Around $b\approx 1$ (about 74 T), the transition probabilities go up, which means dark excitons become bright. At higher temperature, the transition probabilities go up more smoothly. The 74 T is too hard to realize experimentally. Figure 3(c) shows that the critical magnetic field of larger dots with radius of 25 Å, being about 8.4 T, is much smaller. That is because 25 Å is not much smaller than 25.85 Å. We see that as the temperature goes up, the transition probabilities at $b=0$ increase very quickly, which means dark excitons do not become very dark.

C. Circular polarization

Experimentally it is found that the circular polarization factors of the optical transition of randomly oriented dots with radius of 28.5 Å saturate at, about 0.8, other than 1 in magnetic fields.[4] It is very interesting because in zinc-blende case, the saturation value of the circular polarization factors in magnetic fields is 1. We attribute this saturation value of 0.8 to the asymmetry of the crystal structure of CdSe. We represent the dipole transition operators of σ^+, σ^- polarizations as

$$p_x\cos\theta - p_z\sin\theta + ip_y, \tag{18}$$

$$p_x\cos\theta - p_z\sin\theta - ip_y, \tag{19}$$

respectively, where θ is the angle between the orientation of the magnetic field and the z axis of the crystal structure. The orientation of the wave propagation is always along the orientation of the magnetic field. With a given $\cos\theta$ and the optical transition between a given electron state and a given hole state, the intensities of σ^+ and σ^- transitions are proportional to

$$I_{\sigma^+}=\left\{\sum_{l,n,m,s}[a_{l,n,m,s}e_{l,n,m,s}(\cos\theta-1)/2 + d_{l,n,m,s}e_{l,n,m,s}(\cos\theta+1)/2-b_{l,n,m,s}e_{l,n,m,s}\sin\theta/\sqrt{2}]\right\}^2, \tag{20}$$

$$I_{\sigma^-}=\left\{\sum_{l,n,m,s}[a_{l,n,m,s}e_{l,n,m,s}(\cos\theta+1)/2 + d_{l,n,m,s}e_{l,n,m,s}(\cos\theta-1)/2-b_{l,n,m,s}e_{l,n,m,s}\sin\theta/\sqrt{2}]\right\}^2. \tag{21}$$

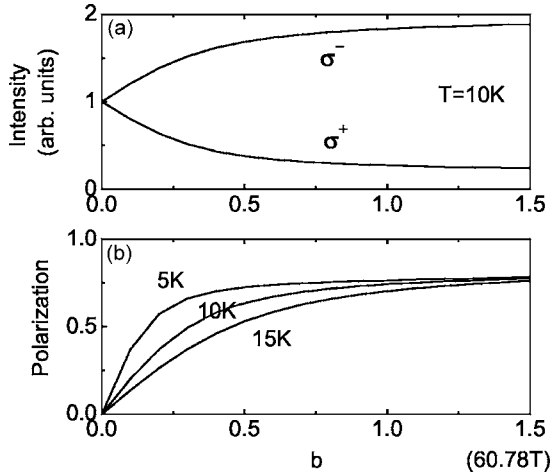

FIG. 4. (a) The normalized intensities of σ^- and σ^+ transitions of dots (28.5 Å) as functions of b. (b) Circular polarization factors of dots (28.5 Å) as functions of b.

Multiply the Boltzmann distribution factor of each state and sum up all the contributions to the intensities. $a_{l,n,m,s}$, $b_{l,n,m,s}$, $d_{l,n,m,s}$, and $e_{l,n,m,s}$ are given in Eqs. (5) and (8).

When $\cos\theta=1$, $I_{\sigma^+}=\{\Sigma_{l,n,m,s}(d_{l,n,m,s}e_{l,n,m,s})\}^2$, $I_{\sigma^-}=\{\Sigma_{l,n,m,s}(a_{l,n,m,s}e_{l,n,m,s})\}^2$, so that $|1,-1\rangle$ and $|1,1\rangle$ in Eq. (1) contribute to σ^+ and σ^- transitions, respectively. The energies of $|1,1\rangle$ and $|1,-1\rangle$ split explicitly due to the antisymmetric Hamiltonian. So the antisymmetric Hamiltonian is very important to the effects of magnetic field on the circular polarization of the optical transition of dots. We sum I_{σ^+} and I_{σ^-} over all orientations, respectively. The normalized intensities of σ^- and σ^+ transitions of randomly oriented dots with radius of 28.5 Å at $T=10$ K as functions of b are shown in Fig. 4(a). The g-factors[14] used here are $g_e=1.138$ and $g_h^*=0.73$. The g-factors of dots with radius of 21 Å (25 Å) and 28.5 Å are from different sources. This does not affect the conclusions. We see that, as the magnetic field increases, the intensity of σ^- transition goes up and the intensity of σ^+ transition goes down. There is no jump of intensity because there is no dark exciton as 28.5 Å $>$ 25.85 Å. Experimentally, the exciton g-factors at this low temperature exhibit values between 0.74 ± 0.05 and 0.87 ± 0.05,[14] which are close to the g-factors of bright exciton states. For the bright exciton states $g_{ex}=1.004-1.5$,[4] which is much smaller than that of the dark states $g_{ex}\approx 4$.[11] This supports that the critical radius is 25.85 Å. We calculate the circular polarization factor by

$$P=(I_{\sigma^-}-I_{\sigma^+})/(I_{\sigma^-}+I_{\sigma^+}). \tag{22}$$

The circular polarization factors of the optical transition of the same dots in Fig. 4(a) as functions of b are shown in Fig. 4(b). We see that the saturation value of the circular polarization factors is not 1, but about 0.8. In the zinc-blend case, the x axis of crystal structure is equivalent to the z axis. When the external magnetic field is applied along the z axis, the saturation value is 1. So when the dots are randomly oriented the saturation value is also 1. In the wurtzite case, the crystal structure is asymmetric from the x axis to the z axis. When the field is applied along the x axis, the dipole transition operators of σ^+ and σ^- are represented as $-p_z+ip_y$, $-p_z-ip_y$, respectively. The minus signs before p_z are due to geometry. As the states with the Z Bloch state go up due to Δ_c, the lowest few states are the states with mainly the X and Y Bloch states. We can calculate the intensities of σ^+ and σ^- transitions by the lowest few states approximately as

$$I_{\sigma^+}=\left\{\sum_{l,n,m,s}(-a_{l,n,m,s}e_{l,n,m,s}/2+d_{l,n,m,s}e_{l,n,m,s}/2)\right\}^2, \tag{23}$$

$$I_{\sigma^-}=\left\{\sum_{l,n,m,s}(a_{l,n,m,s}e_{l,n,m,s}/2-d_{l,n,m,s}e_{l,n,m,s}/2)\right\}^2. \tag{24}$$

We see that $I_{\sigma^+}=I_{\sigma^-}$ and the circular polarization factor is zero. We can give this another explanation. The crystal field splitting energy term is simply written as

$$H_{cs}=\begin{pmatrix}0&0&0\\0&0&0\\0&0&\Delta_c\end{pmatrix}, \tag{25}$$

when the basic functions are X, Y, and Z. If we take the basic functions as $(1/\sqrt{2})(Z+iY)$, X, and $(1/\sqrt{2})(Z-iY)$, H_{cs} is given by

$$H_{cs}=\begin{pmatrix}\frac{1}{2}\Delta_c&0&\frac{1}{2}\Delta_c\\0&0&0\\\frac{1}{2}\Delta_c&0&\frac{1}{2}\Delta_c\end{pmatrix}. \tag{26}$$

The off-diagonal terms in Eq. (26) admix the states with $(1/\sqrt{2})(Z+iY)$ and $(1/\sqrt{2})(Z-iY)$. $(1/\sqrt{2})(Z+iY)$ and $(1/\sqrt{2})(Z-iY)$ contribute to σ^+ and σ^- transitions, respectively, when the field is applied along the x axis. The mixture of $(1/\sqrt{2})(Z+iY)$ and $(1/\sqrt{2})(Z-iY)$ leads to a nearly zero circular polarization factor. The upper two explanations are equivalent. The circular polarization factors of single dots (GaAs and CdSe) with radius of 28.5 Å at $T=10$ K and $b=0.5$ as functions of $\cos\theta$ are shown in Fig. 5. The dashed line represents the GaAs case. The parameters[15] for GaAs used here are $m_e=0.067m_0$, $L=18.4$, $M=3.77$, $N=19.6$, Δ_{so}

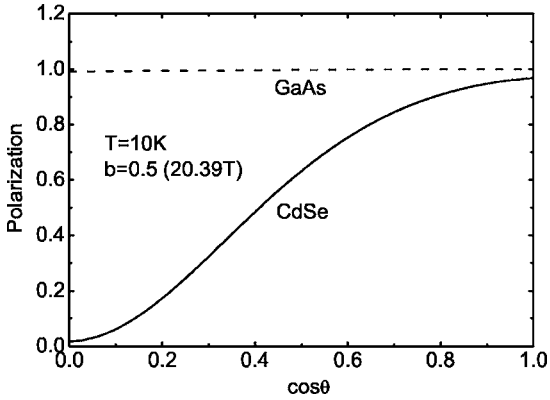

FIG. 5. Circular polarization factors of single dots (28.5 Å) as functions of $\cos\theta$.

=341 meV, g_e=0.44, and g_h^*=1.66. We see that the circular polarization factors are nearly the same from cos θ=0 to cos θ=1. The solid line represents the CdSe case. We see that the circular polarization factors change from nearly 0 to about 1 as cos θ changes from 0 to 1. As a result, it is, in principle, possible to use the polarization spectroscopy to determine the orientation of the z axis of the crystal structure of individual dots.

IV. CONCLUSION

The Hamiltonian of the wurtzite quantum dots in the presence of external homogeneous magnetic field is given. The electron and hole energy levels and wave functions as functions of the magnetic field are obtained. It is found that the hole ground state changes from optically passive state to optically active state under appropriate magnetic field. In the absence of external magnetic field, with Δ_c=25 meV, the dark excitons appear when the radius is smaller than 25.85 Å. This critical radius is different from 30 Å when Δ_c=40 meV. The critical magnetic field under which the dark excitons become bright is dependent sensitively on the radius near 25.85 Å. The circular polarization factors of optical transitions of randomly oriented dots are zero in the absence of external magnetic field and increase with the increase of the magnetic field. The circular polarization factors of single dots change from nearly 0 to about 1 as the orientation of magnetic field changes from the x axis of crystal structure to the z axis, which can be used to determine the orientation of the z axis of the crystal structure of individual dots. The antisymmetric Hamiltonian is very important to the effects of magnetic field on the circular polarization of the optical transition of dots.

ACKNOWLEDGMENTS

This work is supported by the National Natural Science Foundation of China No. 90301007 and the special funds for Major State Basic Research Project No. G001CB3095 of China.

APPENDIX A

In this Appendix we give the forms of the magnetic-momentum Hamiltonians H_{mm_e}, H_{mm_h} and the spin Zeeman splitting terms H_{Zeeman_e}, H_{Zeeman_h}. As $\mathbf{p}\Rightarrow\mathbf{p}+e\mathbf{A}$, $p_\alpha p_\beta \Rightarrow \{p_\alpha p_\beta\}$, the symmetric tensors of momentum operator change into

$$p^2 \Rightarrow p^2 + eB_zL_z - \frac{e^2}{2}B_z^2 r_1^{(1)} r_{-1}^{(1)} - \frac{ie}{\sqrt{2}}B_x(P_1^{(1)} r_0^{(1)} + P_{-1}^{(1)} r_0^{(1)}) - \frac{e^2}{2\sqrt{2}}B_z B_x (r_{-1}^{(1)} r_0^{(1)} - r_1^{(1)} r_0^{(1)}) + \frac{e^2}{4}B_x^2 r_0^{(1)2} + \frac{ie}{\sqrt{2}}B_x(P_0^{(1)} r_1^{(1)} + P_0^{(1)} r_{-1}^{(1)}) - \frac{e^2}{8}B_x^2(r_1^{(1)2} + r_{-1}^{(1)2} + 2r_1^{(1)} r_{-1}^{(1)}), \tag{A1a}$$

$$P_0^{(2)} \Rightarrow P_0^{(2)} + \sqrt{\frac{3}{2}}\left(-eB_zL_z + \frac{e^2}{2}B_z^2 r_1^{(1)} r_{-1}^{(1)}\right) + \sqrt{\frac{3}{2}}\left(\frac{ie}{\sqrt{2}}B_x(P_1^{(1)} r_0^{(1)} + P_{-1}^{(1)} r_0^{(1)}) + \frac{e^2}{2\sqrt{2}}B_z B_x (r_{-1}^{(1)} r_0^{(1)} - r_1^{(1)} r_0^{(1)}) - \frac{e^2}{4}B_x^2 r_0^{(1)2}\right) + \sqrt{\frac{3}{2}}\left(i\sqrt{2}eB_x(P_0^{(1)} r_1^{(1)} + P_0^{(1)} r_{-1}^{(1)}) - \frac{e^2}{4}B_x^2(r_1^{(1)2} + r_{-1}^{(1)2} + 2r_1^{(1)} r_{-1}^{(1)})\right), \tag{A1b}$$

$$P_1^{(2)} \Rightarrow P_1^{(2)} + \frac{3}{\sqrt{2}}ieB_zP_0^{(1)} r_1^{(1)} + \frac{3}{2}ieB_x(P_0^{(1)} r_0^{(1)} + P_1^{(1)} r_1^{(1)} + P_1^{(1)} r_{-1}^{(1)}) - \frac{3}{4}e^2B_zB_x(r_1^{(1)2} + r_1^{(1)} r_{-1}^{(1)}) - \frac{3}{4\sqrt{2}}e^2B_x^2(r_0^{(1)} r_1^{(1)} + r_0^{(1)} r_{-1}^{(1)}), \tag{A1c}$$

$$P_{-1}^{(2)} \Rightarrow P_{-1}^{(2)} - \frac{3}{\sqrt{2}}ieB_zP_0^{(1)} r_{-1}^{(1)} + \frac{3}{2}ieB_x(P_0^{(1)} r_0^{(1)} + P_{-1}^{(1)} r_1^{(1)} + P_{-1}^{(1)} r_{-1}^{(1)}) + \frac{3}{4}e^2B_zB_x(r_{-1}^{(1)2} + r_1^{(1)} r_{-1}^{(1)}) - \frac{3}{4\sqrt{2}}e^2B_x^2(r_0^{(1)} r_1^{(1)} + r_0^{(1)} r_{-1}^{(1)}), \tag{A1d}$$

$$P_2^{(2)} \Rightarrow P_2^{(2)} + 3ieB_zP_1^{(1)} r_1^{(1)} - \frac{3}{2}\frac{e^2}{2}B_z^2 r_1^{(1)2} - \frac{3}{8}e^2B_x^2 r_0^{(1)2} + \frac{3}{2\sqrt{2}}ieB_xP_1^{(1)} r_0^{(1)} - \frac{3}{4\sqrt{2}}e^2B_zB_x r_1^{(1)} r_0^{(1)}, \tag{A1e}$$

$$P_{-2}^{(2)} \Rightarrow P_{-2}^{(2)} - 3ieB_zP_{-1}^{(1)} r_{-1}^{(1)} - \frac{3}{2}\frac{e^2}{2}B_z^2 r_{-1}^{(1)2} - \frac{3}{8}e^2B_x^2 r_0^{(1)2} + \frac{3}{2\sqrt{2}}ieB_xP_{-1}^{(1)} r_0^{(1)} + \frac{3}{4\sqrt{2}}e^2B_zB_x r_{-1}^{(1)} r_0^{(1)}, \tag{A1f}$$

$$P_1^{(1)} \Rightarrow P_1^{(1)} + \frac{1}{2}ieB_z r_1^{(1)} + \frac{i}{2\sqrt{2}}eB_x r_0^{(1)}, \tag{A1g}$$

$$P_{-1}^{(1)} \Rightarrow P_{-1}^{(1)} - \frac{1}{2}ieB_z r_{-1}^{(1)} + \frac{i}{2\sqrt{2}}eB_x r_0^{(1)}. \tag{A1h}$$

$r^{(1)}$ is the first-order tensor of the coordinate operator. Substituting Eq. (A1) into Eqs. (2) and (6) leads to the form of the symmetric part of the Luttinger Hamiltonian, which can be divided into two parts: one contains B_z and B_x, the other does not. We name the former magnetic-momentum Hamiltonian, denoted as H_{mm_e} and H_{mm_h} for the electron and hole, respectively. If the external magnetic field is applied along the z axis of the crystal structure (B_x=0), H_{mm_e}, H_{mm_h} can be written as

$$H_{mm\_e} = \frac{1}{2m_a}\left(eB_zL_z - \frac{e^2}{2}B_z^2 r_+ r_-\right) - \frac{1}{2m_b}\sqrt{\frac{2}{3}}\left(-\sqrt{\frac{3}{2}}eB_zL_z + \sqrt{\frac{3}{2}}\frac{e^2}{2}B_z^2 r_1^{(1)} r_{-1}^{(1)}\right), \tag{A2}$$

$$H_{mm\_h} = \frac{1}{2m_0}H_a, \tag{A3a}$$

$$H_a = \begin{pmatrix}
\gamma_1\left(eB_zL_z - \frac{e^2}{2}B_z^2 r_1^{(1)} r_{-1}^{(1)}\right) & Ap_0\left(-\frac{1}{2}ieB_z r_{-1}^{(1)}\right) & \eta\left(-3ieB_z P_{-1}^{(1)} r_{-1}^{(1)} - \frac{3}{2}\frac{e^2}{2}B_z^2 r_{-1}^{(1)2}\right) \\
-\sqrt{\frac{2}{3}}\gamma_2\left(-\sqrt{\frac{3}{2}}eB_zL_z + \sqrt{\frac{3}{2}}\frac{e^2}{2}B_z^2 r_1^{(1)} r_{-1}^{(1)}\right) & +\sqrt{2}\gamma_3'\left(-\frac{3}{\sqrt{2}}ieB_z P_0^{(1)} r_{-1}^{(1)}\right) & +\delta\left(3ieB_z P_1^{(1)} r_1^{(1)} - \frac{3}{2}\frac{e^2}{2}B_z^2 r_1^{(1)2}\right) \\
-Ap_0\left(\frac{1}{2}ieB_z r_1^{(1)}\right) & \gamma_1'\left(eB_zL_z - \frac{e^2}{2}B_z^2 r_1^{(1)} r_{-1}^{(1)}\right) & Ap_0\left(-\frac{1}{2}ieB_z r_{-1}^{(1)}\right) \\
-\sqrt{2}\gamma_3'\left(\frac{3}{\sqrt{2}}ieB_z P_0^{(1)} r_1^{(1)}\right) & +2\sqrt{\frac{2}{3}}\gamma_2'\left(-\sqrt{\frac{3}{2}}eB_zL_z + \sqrt{\frac{3}{2}}\frac{e^2}{2}B_z^2 r_1^{(1)} r_{-1}^{(1)}\right) & +\sqrt{2}\gamma_3'\left(-\frac{3}{\sqrt{2}}ieB_z P_0^{(1)} r_{-1}^{(1)}\right) \\
\eta\left(3ieB_z P_1^{(1)} r_1^{(1)} - \frac{3}{2}\frac{e^2}{2}B_z^2 r_1^{(1)2}\right) & -Ap_0\left(\frac{1}{2}ieB_z r_1^{(1)}\right) & \gamma_1\left(eB_zL_z - \frac{e^2}{2}B_z^2 r_1^{(1)} r_{-1}^{(1)}\right) \\
+\delta\left(-3ieB_z P_{-1}^{(1)} r_{-1}^{(1)} - \frac{3}{2}\frac{e^2}{2}B_z^2 r_{-1}^{(1)2}\right) & -\sqrt{2}\gamma_3'\left(\frac{3}{\sqrt{2}}ieB_z P_0^{(1)} r_1^{(1)}\right) & -\sqrt{\frac{2}{3}}\gamma_2\left(-\sqrt{\frac{3}{2}}eB_zL_z + \sqrt{\frac{3}{2}}\frac{e^2}{2}B_z^2 r_1^{(1)} r_{-1}^{(1)}\right)
\end{pmatrix}. \tag{A3b}$$

The spin Zeeman splitting terms are written as

$$H_{Zeeman\_e} = \frac{1}{2}g_e\mu_B\sigma\cdot\mathbf{B}, \tag{A4a}$$

$$H_{Zeeman\_h} = \frac{1}{2}g_h\mu_B\sigma\cdot\mathbf{B}. \tag{A4b}$$

APPENDIX B

In this Appendix we give the matrix elements of the tensors $P_\mu^{(2)}$, $P_\mu^{(1)}$, $r_\mu^{(1)}$, $P_\mu^{(1)}r_\nu^{(1)}$, and $r_\mu^{(1)}r_\nu^{(1)}$. We denote the envelope functions $C_{l,n}j_l(k_n^l r)Y_{l,m-1}(\theta,\phi)$ with different n as the same one $|l,m\rangle$. n is only useful to the integration of Bessel functions which is very easy and is not listed here. The nonzero matrix elements are $\langle l+2,m'|P_\mu^{(2)}|l,m\rangle$, $\langle l,m'|P_\mu^{(2)}|l,m\rangle$, $\langle l-2,m'|P_\mu^{(2)}|l,m\rangle$, $\langle l+1,m'|P_\mu^{(1)}|l,m\rangle$, $\langle l-1,m'|P_\mu^{(1)}|l,m\rangle$, $\langle l+1,m'|r_\mu^{(1)}|l,m\rangle$, $\langle l-1,m'|r_\mu^{(1)}|l,m\rangle$, $\langle l+2,m'|P_\mu^{(1)}r_\nu^{(1)}|l,m\rangle$, $\langle l,m'|P_\mu^{(1)}r_\nu^{(1)}|l,m\rangle$, $\langle l-2,m'|P_\mu^{(1)}r_\nu^{(1)}|l,m\rangle$, $\langle l+2,m'|r_\mu^{(1)}r_\nu^{(1)}|l,m\rangle$, $\langle l,m'|r_\mu^{(1)}r_\nu^{(1)}|l,m\rangle$, and $\langle l-2,m'|r_\mu^{(1)}r_\nu^{(1)}|l,m\rangle$. The matrix elements consist of CG coefficients and reduced matrix elements, for example

$$\langle l',m'|P_\mu^{(2)}|l,m\rangle = (-1)^{l'-m'}\begin{pmatrix} l' & 2 & l \\ -m' & \mu & m\end{pmatrix}(l'\|P^{(2)}\|l), \tag{B1}$$

$$\langle l',m'|P_\mu^{(1)}|l,m\rangle = (-1)^{l'-m'}\begin{pmatrix} l' & 1 & l \\ -m' & \mu & m\end{pmatrix}(l'\|P^{(1)}\|l), \tag{B2}$$

$$\langle l',m'|r_\mu^{(1)}|l,m\rangle = (-1)^{l'-m'}\begin{pmatrix} l' & 1 & l \\ -m' & \mu & m\end{pmatrix}(l'\|r^{(1)}\|l), \tag{B3}$$

$$\begin{aligned}\langle l+2,m'|P_\mu^{(1)}r_\nu^{(1)}|l,m\rangle &= (-1)^{l+1-m-\nu}\begin{pmatrix} l+1 & 1 & l \\ -m-\nu & \nu & m\end{pmatrix}(l+1\|r^{(1)}\|l) \\ &\times(-1)^{l+2-m-\nu-\mu}\begin{pmatrix} l+2 & 1 & l+1 \\ -m-\nu-\mu & \mu & m+\nu\end{pmatrix} \\ &\times(l+2\|P^{(1)}\|l+1),\end{aligned} \tag{B4}$$

$$\langle l-2,m'|r_\mu^{(1)}r_\nu^{(1)}|l,m\rangle = (-1)^{l-1-m-\nu}\begin{pmatrix} l-1 & 1 & l \\ -m-\nu & \nu & m \end{pmatrix}(l-1\|r^{(1)}\|l) \times(-1)^{l-2-m-\nu-\mu}\begin{pmatrix} l-2 & 1 & l-1 \\ -m-\nu-\mu & \mu & m+\nu \end{pmatrix} \times(l-2\|r^{(1)}\|l-1) \quad \text{(B5)}$$

The reduced matrix elements are given by

$$(l-2\|P^{(2)}\|l) = -3\sqrt{\frac{l(l-1)}{2l-1}}\left(\frac{d^2}{dr^2}+\frac{2l+1}{r}\frac{d}{dr}+\frac{l^2-1}{r^2}\right), \quad \text{(B6)}$$

$$(l\|P^{(2)}\|l) = \sqrt{3}\sqrt{\frac{l(2l+1)(2l+2)}{(2l-1)(2l+3)}}\left(\frac{d^2}{dr^2}+\frac{2}{r}\frac{d}{dr}-\frac{l(l+1)}{r^2}\right), \quad \text{(B7)}$$

$$(l+2\|P^{(2)}\|l) = -\frac{3}{2}\sqrt{\frac{(2l+2)(2l+4)}{2l+3}} \times\left(\frac{d^2}{dr^2}-\frac{2l+1}{r}\frac{d}{dr}+\frac{l(l+2)}{r^2}\right), \quad \text{(B8)}$$

$$(l+1\|P^{(1)}\|l) = \frac{\hbar}{i}\sqrt{l+1}\left(\frac{d}{dr}-\frac{l}{r}\right), \quad \text{(B9)}$$

$$(l-1\|P^{(1)}\|l) = -\frac{\hbar}{i}\sqrt{l}\left(\frac{d}{dr}+\frac{l+1}{r}\right), \quad \text{(B10)}$$

$$(l+1\|r^{(1)}\|l) = \sqrt{l+1}r, \quad \text{(B11)}$$

$$(l-1\|r^{(1)}\|l) = -\sqrt{l}r. \quad \text{(B12)}$$

[1] Jian-Bai Xia, Phys. Rev. B **40**, 8500 (1989).
[2] Jian-Bai Xia and Jingbo Li, Phys. Rev. B **60**, 11540 (1999).
[3] A. Baldereschi and Nunzio O. Lipari, Phys. Rev. B **8**, 2697 (1973).
[4] E. Johnston-Halperin, D. D. Awschalom, S. A. Crooker, Al. L. Efros, M. Rosen, X. Peng, and A. P. Alivisatos, Phys. Rev. B **63**, 205309 (2001).
[5] M. Paillard, X. Marie, P. Renucci, T. Amand, A. Jbeli, and J. M. Gérard, Phys. Rev. Lett. **86**, 1634 (2001).
[6] K. P. Hewaparakrama, N. Mukolobwiez, L. M. Smith, H. E. Jackson, S. Lee, M. Dobrowolska, and J. Furdyna, cond-mat/0309002.
[7] S. Mackowski, T. Gurung, H. E. Jackson, L. M. Smith, J. K. Furdyna, and M. Dobrowolska, cond-mat/0411036.
[8] J. M. Luttinger, Phys. Rev. **102**, 1030 (1956).
[9] Joshua Schrier and K. B. Whaley, Phys. Rev. B **67**, 235301 (2003).
[10] P. Chen and K. B. Whaley, Phys. Rev. B **70**, 045311 (2004).
[11] Al. L. Efros, M. Rosen, M. Kuno, M. Nirmal, D. J. Norris, and M. Bawendi, Phys. Rev. B **54**, 4843 (1996).
[12] A. V. Rodina, Al. L. Efros, and A. Yu. Alekseev, Phys. Rev. B **67**, 155312 (2003).
[13] Al. L. Efros and M. Rosen, Phys. Rev. B **58**, 7120 (1998).
[14] J. A. Gupta, D. D. Awschalom, Al. L. Efros, and A. V. Rodina, Phys. Rev. B **66**, 125307 (2002).
[15] O. Madelung, *LANDOLT-BŐRNSTEIN*, Volume 17a, Semiconductors: Physics of Group IV Elements and III-V Compounds (Springer-Verlag, Berlin, 1982), p. 220, 222, 223.